doi:10.1038/nature10009

SUPPLEMENTARY FIGURES

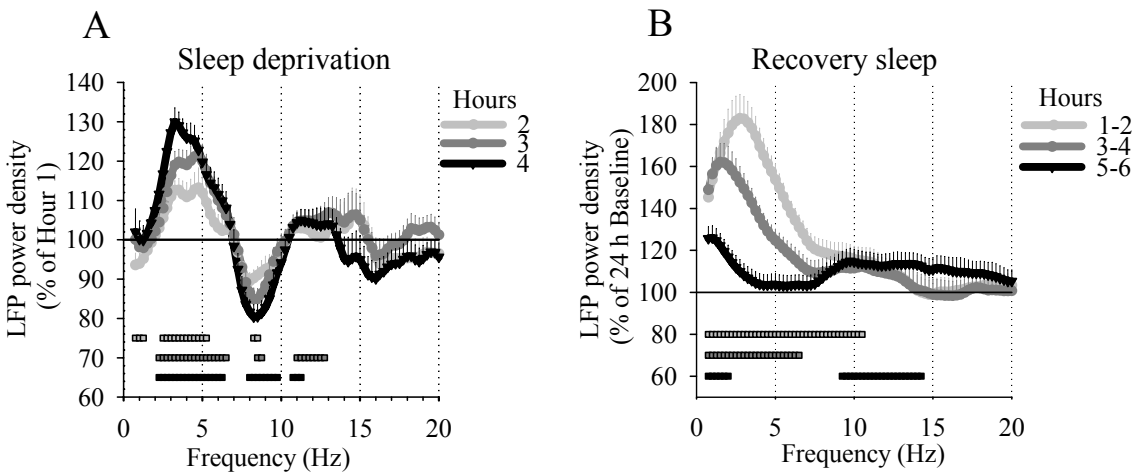

Supplementary Figure 1. Effects of sleep-wake history on wake and sleep LFP power spectra

A. Time course of wake LFP power spectra from the frontal derivation during 4 h of sleep deprivation. Mean values (n=11 rats) + SEM are shown for consecutive 1-h intervals as % of the corresponding first hour of sleep deprivation. Horizontal lines below denote frequency bins where EEG power differed significantly from the first interval ($p<0.05$, paired t-test).
B. Time course of NREM sleep LFP power spectra from the frontal derivation during 6 h of recovery after 4 h of sleep deprivation. Mean values (n=11 rats) + SEM are shown for consecutive 2-h intervals as % of 24-h baseline. Horizontal lines below denote frequency bins where EEG power differed significantly from baseline ($p<0.05$, paired t-test).

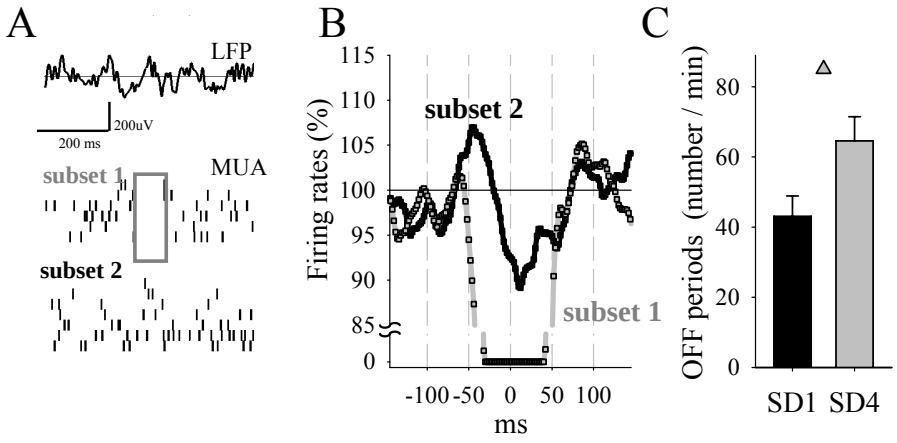

Supplementary Figure 2. Hyper-local OFF periods within a cortical region

A. Hyper-local OFF periods. Top: 600 ms frontal LFP record in wake; bottom: corresponding raster plots of MUA in the frontal cortex recorded from the same microelectrode array, subdivided into two subsets: neurons in subset 2 do not cease firing when all neurons in subset 1 are silent (box=OFF period). Each vertical line is a spike.
B. Population firing rate in subset 1 and subset 2 ± 150 ms from the midpoint of the hyper-local OFF period in subset 1. Values are shown as % of mean firing rates during the preceding 100 ms.
C. Absolute change in the number of hyper-local OFF periods in the frontal derivation during waking from SD1 to SD4. Mean values (n=11 rats) +SEM. Triangle depicts significant difference ($F(1,21)=7.99$, $p=0.0180$, ANOVA).

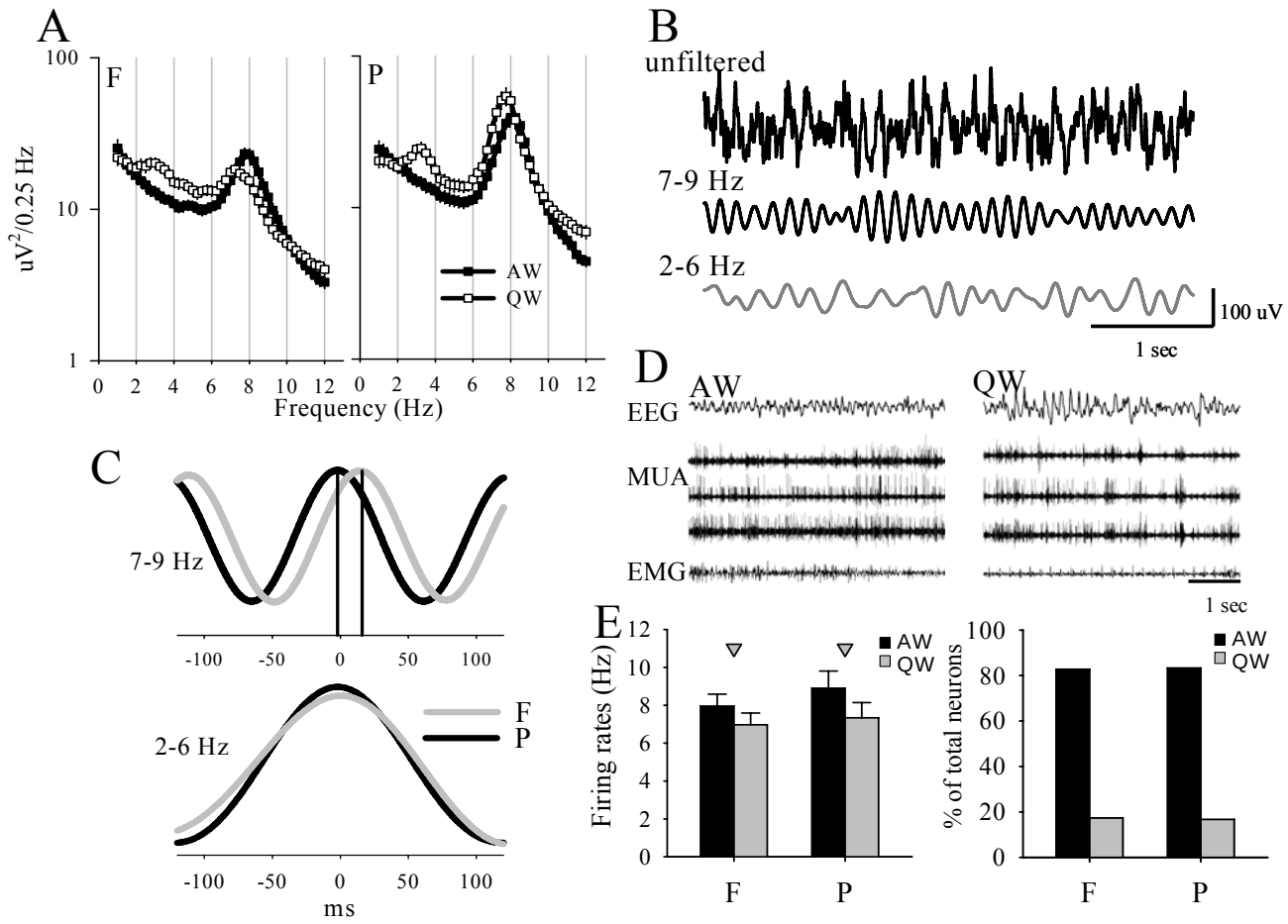

Supplementary Figure 3. Active wake (AW) vs quiet wake (QW): behavior, LFP and neuronal activity

A. Wake LFP power spectra in the frontal (F) and in the parietal (P) derivation during 4 h sleep deprivation. Mean values (n=7 rats) are shown separately for AW and QW. B. 4-s record of wake LFP signal: top, unfiltered, middle: filtered at 7-9 Hz, bottom: filtered at 2-6 Hz. C. Average LFP signals filtered at 7-9 Hz and 2-6 Hz in the frontal (F) and parietal (P) derivation during sleep deprivation, aligned relative to the parietal signal. Note a consistent phase delay for the 7-9 Hz band. D. Cortical EEG, multiunit activity (MUA) and electromyogram (EMG) recorded simultaneously in the same rat from a microwire array placed in the parietal cortex (three individual channels are shown). Typical examples of active waking (AW) and quiet waking (QW) are shown. Note high-amplitude slow / theta waves and prolonged synchronous periods of neuronal silence in QW. E. Left: Average firing rates of cortical neurons in active wake (AW) and quiet wake (QW) in the frontal (F) and parietal (P) derivation. Mean values (n=7 rats) + SEM. Triangles depict significant differences ($P<0.05$, paired t-test). Right: Proportion of neurons showing higher firing rates in active wake (AW>QW) and quiet wake (QW>AW). Mean values (n=7 rats).

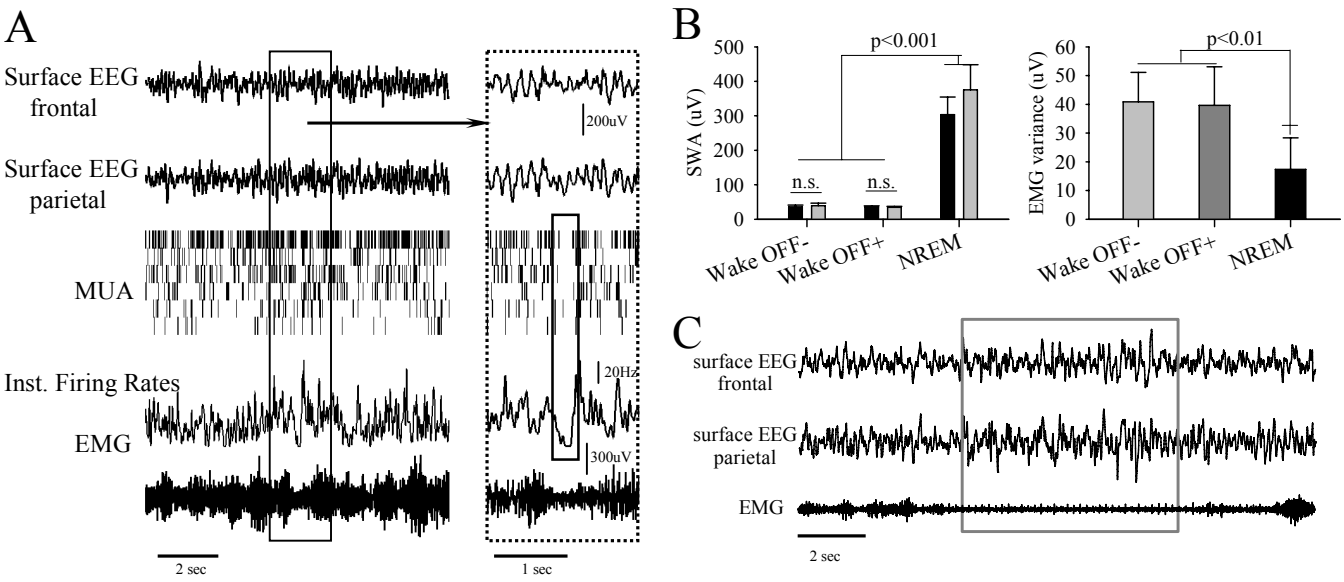

Supplementary Figure 4. Local OFF periods in the wake state

A. Left: A representative 10-s example of an alert wake state. Top: surface EEG signals recorded from the epidural screws mounted above the right frontal and left parietal cortex. Raster plots below the EEG traces depict multiunit spiking activity (MUA), recorded with a microwire array placed intracortically in the left frontal cortex. Each vertical line is a spike. The curve below the raster plots shows instantaneous firing rate of the entire neuronal population computed with Gaussian kernel. Bottom: EMG recorded from the neck muscle. Note that the muscle tone is high, as typical for wakefulness, even during a clear-cut OFF period (boxed). Right: The 2-s record outlined with a box on the left panel centered on the OFF period. B. Left: EEG slow wave activity (SWA) in the frontal (black) and parietal derivation (gray) computed for 4-s wake epochs during which OFF periods were absent (Wake OFF-) or when at least one OFF period was detected (Wake OFF+), and the average SWA during NREM sleep. Note that SWA in wake is similar irrespective of the presence of OFF periods, but significantly increased in NREM sleep. Mean values + SEM, n=11 rats. Right: EMG activity during wake with and without OFF periods and in NREM sleep. Note that EMG activity in wake was similar irrespective of the presence of OFF periods, but significantly reduced in NREM sleep. C. A typical example of a microsleep – short episode of sleep lasting several seconds, characterized by the appearance of surface EEG slow waves in both the frontal and the parietal derivation and a drop of muscle tone (EMG).

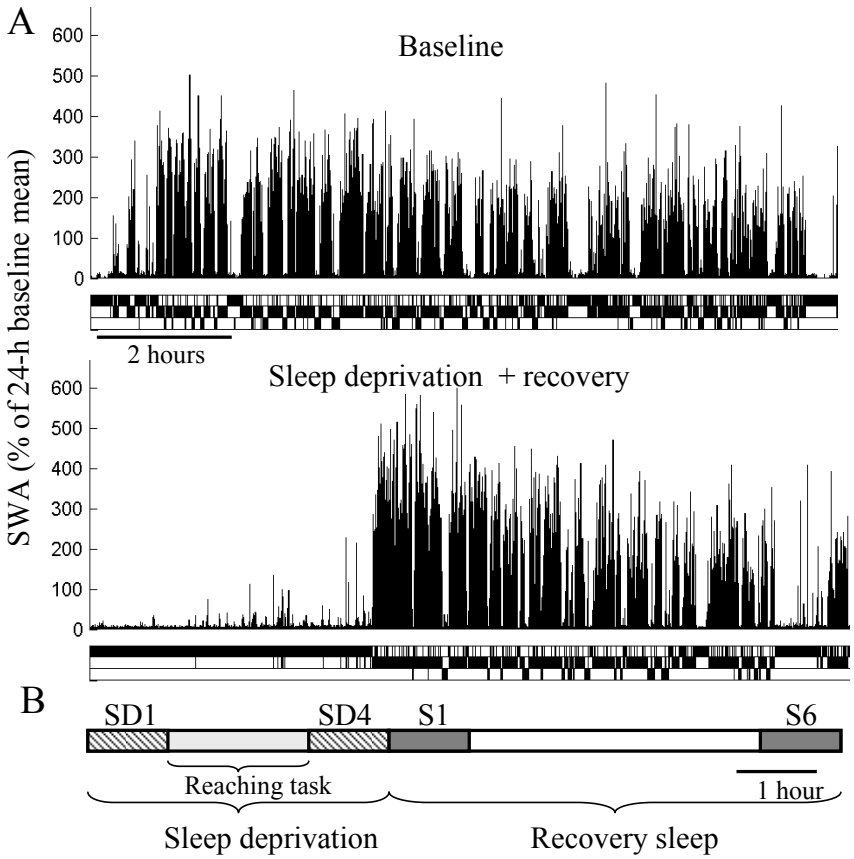

Supplementary Figure 5. Experimental design

A. Top: NREM SWA (% of 24-h baseline mean) and hypnogram of a 10-hour interval starting at light onset during baseline in one representative rat. Bottom: NREM SWA (% of 24-h baseline) and hypnogram of a 10-h interval starting at light onset with 4 h sleep deprivation followed by 6 h of recovery in the same rat. B. Schematic of the experimental design: the 4 h of sleep deprivation start at light onset and consists of two 1-h undisturbed wake periods at the beginning and the end of the procedure (SD1 and SD4) and of one 2-h period in between, when the animal is engaged in the reaching task. Sleep deprivation is followed by 6 h recovery sleep (first and sixth hour are designated as S1 and S6).

SUPPLEMENTARY MOVIES

Supplementary Movie 1. Representative example of a successful reach (hit), where the rat successfully grasps the pellet.
Supplementary Movie 2. Representative example of two consecutive unsuccessful reaches (misses), where the rat fails to grasp the pellets, but knocks them off the shelf. Note that the rat is clearly behaviorally awake throughout both trials.

SUPPLEMENTARY MATERIALS

1. Animals

Adult male WKY rats (total n=13) were used for this study. All rats were housed individually in transparent Plexiglas cages. Lighting and temperature were kept constant (LD 12:12, light on at 10am, 23±1°C; food and water available *ad libitum* and replaced daily at 10am, except during the days when the animals were habituated to or trained in a sugar pellet reaching task (see below).

2. Surgical procedure

All procedures related to animal handling, recording etc. followed the National Institutes of Health Guide for the Care and Use of Laboratory Animals and were in accordance with institutional guidelines. One day before surgery animals received an i.p. dose of dexamethasone (0.2mg/kg) to suppress local immunological response [1,2]. Under deep isoflurane anesthesia (1.5-2 % volume), polyimide-insulated tungsten microwire arrays were implanted in the frontal cortex (B: +1-2 mm, L: 2-3 mm, n=11) and/or in the contralateral parietal cortex (B: -2-3 mm, L: 4-5 mm, n=9). The side of implantation was determined prior to surgery after the preferred paw of each animal was determined (see below). The frontal array was always implanted in the motor cortex contralateral to the preferred paw. The arrays were 16-ch (2 rows each of 8 wires) polyimide-insulated tungsten microwire arrays (Tucker-Davis Technologies Inc (TDT), Alachua, FL, wire diameter 33µm, electrode spacing 175-250µm, row separation L-R: 375-500µm; D-V: 0.5mm), and were implanted according to the "Surgical implantation guidelines" (Neuronexus Technologies, Inc.) and [3]. Dexamethasone (0.2mg/kg) was given with food pellets every day for the duration of the experiment.

The surgical procedure was performed in sterile conditions, using Ethylene Oxide sterilized materials. An ~ 2x2 mm craniotomy was made using first a 1.4 mm drill bit and then a 0.5 mm drill bit, with the aid of a high-speed surgical drill. The hole was adjusted to the size of the array by removing the remaining fragments of the bone with a Friedman-Pearson Rongeur (part number 16221-14, FST). In most cases the removal of the dura did not cause bleeding (when bleeding occurred, it was stopped with gelfoam soaked in sterile saline). The dura was dissected with vitrectomy scissors (2.2 mm straight blades, part number 15036-14, FST).

The electrode array was advanced into the brain tissue by penetrating the pia mater, making an effort to avoid vascular damage [4]. Electrode insertion was achieved by advancing the electrode array until both rows of the arrays were at the level of deep cortical layers (~1.5 mm below the pial surface). The final position of the array was adjusted by withdrawing or lowering it

slowly (~50 μm steps) until most channels showed robust single- or multiunit activity. At this stage special care was taken to avoid displacing the array in the horizontal dimension. The two-component silicon gel (KwikSil; World Precision Instruments, FL, USA) was used to seal the craniotomy and protect the surface of the brain from dental acrylic. After ~10 min, required for the gel to polymerize, dental acrylic was gently placed around the electrode, fixing the array to the skull. EEG screws were placed in the frontal and parietal cortex contralateral to the corresponding arrays. The ground and reference screw electrodes were placed above the cerebellum and additional anchor screws were placed in the frontal bone.

3. Signal processing and analysis

Data acquisition and online spike sorting were performed with the Multichannel Neurophysiology Recording and Stimulation System (TDT). Spike data were collected continuously (25 kHz, 300 Hz - 5kHz), concomitantly with local field potentials (LFPs) from the same electrodes (256 Hz, 0.1-100 Hz) and surface EEGs (256 Hz, 0.1-100 Hz). The online spike sorting was performed with OpenEx software (TDT), by applying a voltage window through which the signal had to pass. Amplitude thresholds for online spike detection were set manually based on visual and auditory control and allowed only crossings of spikes with peak amplitude exceeding -25μV (see below). Such thresholding allowed excluding the low amplitude background activity and most of high amplitude artifacts related to chewing and grooming. Whenever the recorded voltage exceeded a predefined threshold (at least -25 μV), a segment of 46 samples (0.48 ms before, 1.36 ms after the threshold crossing) was extracted and stored for later use together with the corresponding time stamps. Spike data were then subjected to offline sorting procedure (see below).

The LFP power spectra during sleep deprivation and subsequent recovery were computed by a Fast Fourier Transform (FFT) routine for 4-sec epochs (Hanning window, 0.25 Hz resolution). As expected, low frequency LFP power increased in wake during sleep deprivation and decreased in NREM sleep during recovery (Supplementary Fig. 1), and the latter changes were more pronounced [5,6]. For further analyses, two frequency bands were selected: high delta / low theta band (2-6 Hz) in wake and slow-wave activity (0.5-4.0 Hz, SWA) in NREM sleep (Supplementary Fig. 1). Detection of individual waves in wake and NREM sleep was performed on the LFP signal after band pass filtering (2-6 and 0.5-4 Hz respectively) with MATLAB filtfilt function exploiting a Chebyshev Type II filter design (MATLAB, The Math Works, Inc., Natick, MA) [7]. Waves were detected as positive deflections of the filtered LFP signal between two consecutive positive deflections above the zero-crossing[8]. Subsequently local and global waves were identified as detailed below.

4. Scoring vigilance states and behavioral analysis

Prior to spectral analysis, wave detection or analysis of neuronal activity, vigilance states were identified for consecutive 4-s epochs. To do so, signals were loaded with custom-written Matlab programs using standard TDT routines, and subsequently transformed into the European Data Format (EDF) with Neurotraces software (www.neurotraces.com). Sleep stages were scored offline by visual inspection of 4-sec epochs (SleepSign, Kissei), where the EEG, LFP, EMG and spike activity were displayed simultaneously. Wake was characterized by low voltage, high frequency EEG pattern and high amplitude, phasic EMG activity (Supplementary Figs. 3,4). Epochs of eating, drinking and intense grooming were carefully excluded (< 5%), since during those periods MUA is contaminated by movement artifacts, for example due to chewing, precluding reliable isolation of individual spikes. NREM sleep was characterized by the occurrence of high

amplitude slow waves and low tonic EMG activity [6,9]. During REM sleep the EEG/LFP was similar to that during wake, but only heart beats and occasional twitches were evident in the EMG signal. During sleep deprivation very short (usually <5 s) events characterized by high-amplitude slow waves in the surface EEG and by low EMG activity (typical of NREM sleep), preceded and followed by behavioral and electrographic signs of wakefulness, were sometimes observed (Supplementary Fig. 4C). Such microsleep episodes occurred at a frequency of 1.75±0.22 / 1 h, were scored as NREM sleep, and as such they were always excluded from the analysis of wakefulness.

Wake is not a homogenous state, therefore it is crucially important to perform analyses *within* substates as similar as possible. The average wake EEG power spectrum is characterized by a prominent peak at ~7-9 Hz and lower but substantial power in lower frequencies (Supplementary Fig. 3A). However, during wake the EEG spectra of individual epochs vary substantially depending on the ongoing behavior (Supplementary Fig. 3A,B). Specifically, fast theta activity (7-9 Hz) is high during active wake (AW), whereas quiet wake (QW) is often characterized by slower waves at high delta – slow theta (2-6 Hz) frequency (Supplementary Fig. 3A,B). We define AW as a state when the animal is moving around the cage while exploring, foraging etc. QW is a state when the animal is alert, with eyes open, readily responds to stimuli, maintains vigilance and posture, but is immobile. Of note, fast theta activity is also often present during QW (Supplementary Fig. 3A), consistent with earlier observations in different species [10,11]. This activity can be related to orienting or attention without overt locomotor activity. The fast (7-9 Hz) and slow (2-6 Hz) activities during wake likely originate from different sources and have different physiological significance [12-16]. The different origin of the two activities was also suggested by our analyses, which showed consistent phase delay (by ~16 ms) of the frontal relative to the parietal 7-9 Hz waves, but not of the 2-6 Hz waves (Supplementary Fig. 3C). Cortical neuronal activity in both derivations also differed markedly between behavioral states (Supplementary Fig. 3D,E), with more neurons discharging at higher rates in AW than in QW.

Since the primary aim of our study was to investigate the effects of sleep/wake history on spontaneous (not behavior-driven) LFP and neuronal activity, we focused our analyses on quiet wake. To do so, we carefully selected 5-10 min of artifact-free QW at the beginning of 4 h of sleep deprivation (hour 1, SD1) and at the end (hour 4, SD4) (Supplementary Fig. 5). The selection was performed based on video recording, LFP, surface EEG and EMG viewed simultaneously. The surface EEG and LFP signals in QW is undoubtedly “wake”, as it is characterized by mainly low voltage activity with theta waves and no slow waves typical for sleep (Supplementary Fig. 3,4). Rearing, grooming, eating or drinking were carefully excluded from the analyses. Thus, the QW state we selected was not confounded by any other behavior and brain activity was mostly spontaneous. On average 12.6 ±1.4 min of QW/rat were used for the analysis of the LFP and neuronal activity. Similarly, for NREM sleep during recovery, the longest episode was selected for each 1-hour interval. The average amount of NREM sleep for S1 and S6 was 28.2 ± 4.1 min.

5. Experimental design

About one week was allowed for recovery after surgery, and experiments were started only after the sleep/wake cycle had fully normalized, as evidenced by the entrainment of sleep and wake by the light/dark cycle and the homeostatic time course of SWA (Supplementary Fig. 5). After stable baseline, animals were recorded during 4 h of sleep deprivation (2-4 experiments per rat, at least 5 days apart), each followed by an undisturbed recovery period (Supplementary Fig. 5).

Sleep deprivation began at light onset and involved continuous observation of the animal and its polysomnographic recording. Prolonged wakefulness for 4 h was achieved by providing the rats with novel objects because this method is effective, ethologically relevant, and does not appear to stress the animals [8,17-19]. Prior to the experiment rats were well habituated to the experimenter and to the exposure to novel objects (exposure at light onset for 30 min/day for several days; new objects every day). Novel objects included nesting and bedding material from other rat cages, wooden blocks, small rubber balls, plastic, metallic, wooden, or paper boxes and tubes of different shape and color. Using other less ecologically relevant paradigms for sleep deprivation, such as touching the rats with a painter's brush, delivering auditory or visual stimuli, or forcing the rats to move at fixed intervals is more stressful and less efficient. At the beginning objects were provided every 10-15 min but as prolonged wakefulness progressed, more frequent interventions were sometimes required (every ~ 5 min). During the procedure, the animals appeared not stressed, they were readily exploring the objects, never engaged in freezing or aggressive behavior, and showed no signs of physical discomfort. Only 6.0±1.6 min of NREM sleep (number of sleep attempts: 20.3±6.2) occurred during the 4 h of sleep deprivation. In each animal one of the sleep deprivation experiments was assigned to be combined with the sugar pellet reaching task [20,21] (see below). Video recordings were performed continuously with infrared cameras (OptiView Technologies, Inc) and stored in real time with 25 frames/sec resolution.

6. Sugar pellet reaching task

To investigate potential consequences of local neuronal 'tiredness' on wake MUA and the LFPs rats were trained on a sugar pellet reaching task [20]. Learning the reaching task engages a circumscribed cortical area within the motor cortex, leads to local plasticity in wake [22], and to increased NREM SWA during subsequent sleep [20,23].

Prior to surgery, rats were first exposed to 45-mg dustless precision sucrose pellets (Bioserve Inc., Frenchtown, NJ) in their home cage to familiarize them with the novel food, and then habituated to the reaching chamber. The reaching chamber (34 x 13 x 24 cm) had a 1 cm-wide vertical opening in the front wall through which a 2 cm wide shelf, mounted 3 cm from the bottom of the chamber on the outside of the front wall, could be accessed. The shelf had two indentations centered on the 1 cm opening in the front wall of the reaching chamber for placement of sucrose pellets. The shelf indentations were placed such that only the contralateral paw could access the sucrose pellet [21]. During training the reaching chamber was placed inside the home cage, so that rats were never removed from their cages and polysomnographic and MUA recordings were never interrupted.

The determination of preferred paw occurred prior to surgery. Rats were food restricted to 85-90% of their free feeding weight (water was provided *ad libitum*) for 1-2 days before habituation began. First, sucrose pellets were sprinkled on the floor and shelf of the chamber. Once animals were familiarized to the chamber, sucrose pellets were placed only in the indentations on the shelf and the preferred limb for reaching was determined. Subsequently, rats were allowed several days with food *ad libitum* before they underwent surgical procedure.

Three-four days prior to the sleep deprivation experiment combined with the reaching task, the rats were again placed on a food restricted regimen, and exposed daily to the reaching chamber. The day of sleep deprivation, rats were mostly awake before light onset (total wake time during the 2-hour interval before light onset was 86.9±5 min). During the first 30-60 min of sleep deprivation (on average 47.6±6.0 min) the animals were kept awake under continuous visual observation in order to collect sufficient amount of artifact-free stable QW epochs for subse-

quent analysis (SD1, Supplementary Fig. 5). The training occurred within subsequent ~ 2h period and consisted of shaping a rat to approach the opening in the front of the chamber, determine whether a pellet was available on the shelf and, if one was present, to reach through the opening and retrieve it with its preferred paw (Supplementary Fig. 5). Following an attempt to obtain a pellet, whether successful or not, rats were required to go to the back of the chamber and approach the front again before another pellet was presented. This sequence of behaviors, defined as a trial, forced the rat to reposition its body to obtain a sucrose pellet. A trial was considered completed every time a rat made an attempt to retrieve a pellet, whether or not it was successful (Supplementary Movies 1 and 2). Thus, consuming a pellet or knocking it off the shelf would both be considered the endpoint of a trial. A reach was defined as the use of the preferred paw to reach through the opening in the front wall in an attempt to obtain a pellet. Successes were defined as a successful retrieval and consumption of a pellet with the preferred paw, regardless of the number of reach attempts. The animals were continuously awake for the duration of the 2-h interval, most of which they spent performing the task. The animals were highly variable in the number of trials and the amount of pellets they retrieved (mean values ± SEM, trials: 153.2±41.6, reaches: 369.7±93.9, pellets: 60.8±12.1). After the task was completed, another 30-60 min of spontaneous undisturbed wake recording were collected (SD4, Supplementary Fig. 5).

In a subset of animals (total n=8), a detailed analysis of video recordings during the reaching task was performed. Digital video recordings were collected synchronously with the recordings of MUA and analyzed frame-by-frame offline with 40-ms resolution. Each reaching attempt was assigned as 'hit' or 'miss' depending on successful or unsuccessful outcome, respectively. Subsequently, MUA data for the preceding 2 s were extracted and analyzed as detailed below. In order to investigate the relationship between the incidence of the OFF periods and behavioral performance, all trials for each individual rat were grouped into two subsets with at least one OFF period and without OFF periods before the grasping attempt.

In humans, sleep deprivation results in an inability to maintain stable level of performance over time as measured in a sustained vigilance task [24]. In our experiment, as a measure of behavioral stability we used the pattern of the occurrence of hits and misses during the period when the rat was performing the task. Specifically, we computed "clusters" of failures, defined as groups of consecutive misses occurring in a row, and determined their average duration. In order to assess how behavioral stability changes across time during the task, we then computed the variance of the cluster durations within the first, intermediate and last 33% of all trials.

7. Detection of local and global OFF periods

In naturally sleeping animals extracellular recordings in the visual or somatosensory neocortex reveal periods of synchronous activity among neuronal populations, interrupted by periods of population silence of variable duration (e.g. [9,25,26]). Consistently, we observed similar periods of generalized neuronal activity (ON periods) and silence (OFF periods) in our recordings from the frontal and parietal cortex (e.g. Fig. 1). As a first step, we asked whether population firing in awake behaving animals shows transient episodes of reduced spiking on a time scale of hundreds of milliseconds, similar to the OFF periods observed during sleep. To compute instantaneous firing rates, we performed a convolution between a Gaussian kernel g(t) and raw spike trains. Spike trains are defined as time series s(t), where positive integer values represent the number of spikes occurring at any time step. The Gaussian kernel was instead defined as:

$$g(t) = \frac{1}{\sqrt{2\pi\sigma^2}} e^{-\frac{(t-\tau)^2}{2\sigma^2}},$$

where σ is the standard deviation and τ is the value around which the Gaussian kernel is centered. We set σ at 25 ms. The instantaneous firing rate f is then computed as:

$$f(t) = \int_0^T s(\tau) g(t-\tau) d\tau$$

Putative OFF periods were defined as troughs on the convoluted signal (top 10% of the troughs below the median instantaneous firing rate). Computing the changes in the number of such OFF periods from SD1 to SD4 revealed a significant increase from 30.4±3.5 to 47.7±5.4 per 1 min ($p<0.05$). Since the sugar pellet reaching task required continuous intense locomotion, complete neuronal silence was rarely observed in the frontal motor cortex during the task. Therefore, in order to investigate the relationship between the local occurrence of OFF periods and behavioral performance, OFF periods were defined as periods of suppressed neuronal activity based on instantaneous population firing rates.

Based on this result, as a next step, we computed the number of OFF periods as periods of total neuronal silence for most of the remaining analyses. All time stamps corresponding to individual detected spike occurrences were concatenated across all recording channels showing robust single- or multiunit activity. Next, onset and offset of the periods with no unit activity were identified. In order to empirically determine the duration of an OFF period in a given neuronal population, and to verify that such OFF periods do not simply arise as a result of variability of firing patterns, we performed simulations of the population firing rates. To take into account a refractory period and/or burstiness we used a renewal process (gamma distribution)[27]. In the gamma distribution two parameters need to be specified: order k and scale factor (1/firing rate). Both parameters were fitted to the data employing maximum likelihood estimation. First we built surrogate spike train data based on the average firing rates. Then we computed the distribution of durations of all OFF periods of any length by fitting a gamma distribution to simulated data. To define a threshold for detecting OFF periods we computed the 99th percentile in the gamma distribution fitting simulated data, and verified whether the number of measured OFF periods exceeding the threshold was significantly higher than 1%. This threshold allowed finding which fraction of the OFF periods from the distribution is significantly longer than what can be expected to occur by chance given the average firing rate of the neuronal population. The average fraction was ~8-10% of total OFF periods in wake (mean duration ~ 85 ms) and ~ 13-14% in NREM sleep (mean duration ~135ms). The average duration of OFF periods in wake was shorter than the duration of OFF periods during sleep, consistent with the fact that sleep deprivation-induced changes in LFP spectral power encompassed a faster frequency band in wake (2-6 Hz) compared to sleep (0.5-4 Hz). The minimal duration of an OFF period within the corresponding fraction was taken as a duration criterion for detecting OFF periods for each individual animal. Importantly, both fractions were significantly higher than 1%.

OFF periods occur not only simultaneously across the entire cortical surface but can be restricted to local cortical areas. In order to investigate local and global occurrence of the OFF periods, in most animals (n=7) we recorded MUA not only in the frontal or parietal derivation, but also in both derivations simultaneously. Subsequently, we detected the OFF periods in each of the two derivations separately, as described above, and quantified those cases where the beginning or the end of the OFF period in one derivation overlapped with the beginning or the end of the OFF periods in the other derivation. If the OFF periods occurred nearly-simultaneously in the two derivations they were called global OFF periods, while the remaining instances were called local OFF periods. In order to verify that global OFF periods are not simply accounted for by the simultaneous and random occurrence of local OFF periods in both cortical areas, we employed a simulation-based approach. The number of occurrences of OFF periods in a certain time

window can be modeled as a Poisson process based on the firing rate of the neuronal population; in a short recording session such process can be considered homogeneous. Therefore, we modeled the occurrence of OFF periods using an exponential distribution based on experimentally determined lag times between consecutive OFF periods and their empirically determined duration. For each experimental condition, we computed the maximum likelihood parameters for exponential distributions of both duration and lags of the local OFF periods. Using the extracted parameters, we generated random numbers according to exponential distributions for both OFF period lags and durations and simulated local OFF periods time series, with the same duration as in the experimental data. We then computed global OFF periods from simulated data and repeated the simulations ten times in order to generate sufficient data for estimating the average number of chance OFF periods and ensure reproducibility of the results. Invariably, we found that the number of the global OFF periods in the original data set was significantly higher than the number of OFF periods in the simulated data set (wake, experimental data: 7.6±1.6 / 1 min, simulated: 3.1±0.7 / 1 min, $F(1,21)= 76.1265$, $p=0.0129$; sleep: experimental data: 37.2±5.6 / 1 min, simulated: 25.2±3.9 / 1 min, $F(1,21)= 157.14$, $p=0.0063$; n=7 rats, 1-3 sleep deprivations / rat, fixed-effects model ANOVA). These results suggest that global OFF periods cannot be simply accounted for by the simultaneous and random occurrence of local OFF periods in both cortical areas.

Finally, we asked whether nearby neurons *within* the same region can enter OFF periods independently. In order to compute such OFF periods ("hyper-local OFF periods", Supplementary Fig. 2A) we subdivided all units within a region into two subpopulations of equal size based on their firing rates, in such a way that the proportion of slow spiking and fast spiking neurons was similar between the two subpopulations, resulting in similar average firing rates (n.s.). We observed that in wake, when one subpopulation decreased firing, the second subpopulation increased firing transiently and then decreases by ~ 15% with a short delay (Supplementary Fig. 2B). In contrast, in NREM sleep when one subpopulation stopped firing, the remaining subset in most cases decreased firing substantially (~50%).

8. Detection and analysis of 2-6 Hz waves in wake and slow waves in NREM sleep

In order to investigate the relationship between neuronal OFF periods and the local LFP, individual waves were detected and analyzed during sleep deprivation and during recovery sleep. Detection of individual waves was performed on the LFP signal after band pass filtering (wake: 2-6 Hz, stopband edge frequencies 1-8 Hz; NREM sleep: 0.5-4 Hz, stopband edge frequencies 0.1-8 Hz) with MATLAB filtfilt function exploiting a Chebyshev Type II filter design (MATLAB, The Math Works, Inc., Natick, MA) [7,8,28]. Waves in both sleep and wake were detected as positive deflections of the filtered LFP signal between two consecutive negative deflections below the zero-crossing. During sleep, the first segment of the wave (from the first negative peak to the maximal positive peak) is thought to correspond to the DOWN state of the slow oscillations, whereas the second segment (from the maximal positive peak to the second negative peak) roughly corresponds to the UP state [7,9,29-33]. The peak-to-peak amplitude of the first and second segment of the wave was computed for each individual wave. All waves were sorted into five amplitude percentage ranges (20 percentiles each) according to the amplitude of the peak (from zero-crossing to maximum positive value) [8] and the largest waves (e.g. 5th percentile) were selected for the final analyses (Figs. 1-2). Similar results in both sleep and wake were obtained when all waves above the median amplitude were considered. In addition, in order to investigate the direct phase relationship between the population OFF periods and LFP waves, averages of

MUA triggered by the LFP waves were computed [9,25,32,34]. To do so, all spike occurrences were aligned to the positive peak of the LFP wave and averaged. We found that not only in sleep but also in wake, high amplitude (5th percentile) positive LFP waves were associated with a significant suppression of unit activity.

We observed in all animals that the individual 2-6 Hz LFP waves have variable shape – some of them are monophasic, and some have a biphasic shape, i.e. the positive peak is followed by a pronounced negative deflection. In order to investigate whether these two kinds of waves are differently affected by sleep deprivation, we separately detected monophasic LFP waves (symmetrical wave-shape, with <25% difference in the peak-to-peak amplitude of up- and down-swings) from biphasic LFP waves (asymmetrical wave-shape, the peak-to-peak amplitude of the down-swing is larger than the peak-to-peak amplitude of the up-swing by at least 25%). Invariably, both types of wake LFP waves increased significantly from SD1 to SD4 ($p<0.01$).

In order to analyze local and global occurrence of LFP waves, we analyzed the signals as above in both the frontal and parietal derivation. Subsequently, "global waves" were defined as events where the beginning or the end of the wave in one derivation overlapped with the beginning or the end of the wave in the other derivation; the remaining, isolated waves were termed "local waves".

9. Spike sorting

Since our study investigated periods of generalized suppression of neuronal activity or total neuronal silence, and did not address firing rates of individual isolated neurons, spike sorting was performed primarily to eliminate artifactual waveforms caused by electrical or mechanical noise. Spikes were detected as events exceeding a threshold usually set at -25 μV[35], which corresponded in most cases to approximately 2 times the average amplitude of background activity (-13.3±3.7μV). Principal components (PCs) were extracted [36] and clustering was performed based on the split and merge expectation maximization (SMEM) algorithm [35,37,38]. This algorithm operates on Gaussian mixtures by iteratively splitting and merging Gaussian clusters, until convergence of a maximization index (likelihood function) is reached. This algorithm is able to estimate the correct number of Gaussian components that, when fitted to the dataset via an expectation maximization (EM) procedure, maximizes the likelihood function. To obtain a satisfactory clustering quality, parameters were initialized as follows: 1) the number of PCs was set to 3, accounting on average for ~70% of the total variance; 2) the thresholds for the convergence of the EM steps was set to 10^{-6}; 3) the threshold th_c for classification was set to 2.5%, i.e. all spikes whose features fell in the tails of Gaussian clusters (0 to th_c and 100-th_c to 100 percentiles) were discarded. The clustering procedure was repeated several times and the outcome with the lowest Bayesian Information Criterion (BIC) was selected; BIC was computed as in [35] on a validation subset of spikes (corresponding to 10% of all spikes), which was the same for all runs of the algorithm. Moreover, an index for isolation quality was computed for each cluster. A set of 10^6 points was randomly extracted from the Gaussian mixture probability distribution and each point was assigned to a cluster. The rate of false positive and false negative occurrences was then computed (quality of isolation index). Clusters having this index large than 0.05 were discarded, since they represented badly isolated sources of detected activity. Post hoc, we also discarded all clusters having an average waveform not resembling a typical extracellular action potential; occasionally some clusters were merged after visual inspection of both waveforms and PC scatterplot revealed non-correct clustering. On average 14.6±1.1 putative neurons were identified per rat per recording day in the frontal derivation. Corresponding numbers for the parietal derivation

were 11.1±1.3. All the recorded units were stable over the 10 h period of recording (4 h sleep deprivation + 6 hours of recovery sleep). The mean absolute difference between the spike amplitude of the first and last 20% percentiles of spikes was only 3.8 ms ± 5.9 ms (std. dev.).

10. Statistical analysis

The absolute values of the measured variables (number of OFF periods and LFP waves) varied across animals. In addition, in some individuals more than one sleep deprivation was performed. To take into account both repeated measurements of the same variable and sample size, we employed fixed-effects model statistics, which provides unbiased estimates. The general model employed was:

$Y_{it} = \alpha_i + \beta i X_{it} + \varepsilon_{it}$,

where the subscripts i and t represent, respectively, the ith animal and the time/condition of measurement, X is the independent variable, Y is the dependent variable, α is the intercept term, β is the angular coefficient term and ε is the error term. This linear model allowed considering cases where both the intercept (i.e. the absolute value) and the slope (i.e. the dependence between independent and dependent variables) depend on individual animals. All statistical analyses were performed in MATLAB.

11. Histological verification

Upon completion of the experiments the position of the LFP electrodes was verified by histology in all animals. After perfusion under deep isoflurane anesthesia (3% in oxygen), brains were post-fixed, rapidly frozen on dry ice, cut into 50µm serial coronal sections, and subjected to cresyl-violet (Nissl) staining. In all cases both rows of the array were located within deep layers (layers V-VI).

REFERENCES

1 Spataro, L. *et al.*, Dexamethasone treatment reduces astroglia responses to inserted neuroprosthetic devices in rat neocortex. *Exp Neurol* 194 (2), 289-300 (2005).

2 Zhong, Y. & Bellamkonda, R.V., Dexamethasone-coated neural probes elicit attenuated inflammatory response and neuronal loss compared to uncoated neural probes. *Brain Res* 1148, 15-27 (2007).

3 Kralik, J.D. *et al.*, Techniques for long-term multisite neuronal ensemble recordings in behaving animals. *Methods* 25 (2), 121-150 (2001).

4 Bjornsson, C.S. *et al.*, Effects of insertion conditions on tissue strain and vascular damage during neuroprosthetic device insertion. *J Neural Eng* 3 (3), 196-207 (2006).

5 Franken, P., Dijk, D.J., Tobler, I., & Borbely, A.A., Sleep deprivation in rats: effects on EEG power spectra, vigilance states, and cortical temperature. *Am J Physiol* 261 (1 Pt 2), R198-208 (1991).

6 Leemburg, S. *et al.*, Sleep homeostasis in the rat is preserved during chronic sleep restriction. *Proc Natl Acad Sci U S A* in press (2010).

7 Achermann, P. & Borbely, A.A., Low-frequency (< 1 Hz) oscillations in the human sleep electroencephalogram. *Neuroscience* 81 (1), 213-222 (1997).

8 Vyazovskiy, V.V., Riedner, B.A., Cirelli, C., & Tononi, G., Sleep homeostasis and cortical synchronization: II. A local field potential study of sleep slow waves in the rat. *Sleep* 30 (12), 1631-1642 (2007).

9 Vyazovskiy, V.V. *et al.*, Cortical firing and sleep homeostasis. *Neuron* 63 (6), 865-878 (2009).

10 Kramis, R., Vanderwolf, C.H., & Bland, B.H., Two types of hippocampal rhythmical slow activity in both the rabbit and the rat: relations to behavior and effects of atropine, diethyl ether, urethane, and pentobarbital. *Exp Neurol* 49 (1 Pt 1), 58-85 (1975).

11 Vanderwolf, C.H., Hippocampal electrical activity and voluntary movement in the rat. *Electroencephalogr Clin Neurophysiol* 26 (4), 407-418 (1969).

12 Petsche, H. & Stumpf, C., Topographic and toposcopic study of origin and spread of the regular synchronized arousal pattern in the rabbit. *Electroencephalogr Clin Neurophysiol* 12, 589-600 (1960).

13 Whishaw, I.Q. & Vanderwolf, C.H., Hippocampal EEG and behavior: changes in amplitude and frequency of RSA (theta rhythm) associated with spontaneous and learned movement patterns in rats and cats. *Behav Biol* 8 (4), 461-484 (1973).

14 Robinson, T.E., Hippocampal rhythmic slow activity (RSA; theta): a critical analysis of selected studies and discussion of possible species-differences. *Brain Res* 203 (1), 69-101 (1980).

15 Leung, L.W. & Borst, J.G., Electrical activity of the cingulate cortex. I. Generating mechanisms and relations to behavior. *Brain Res* 407 (1), 68-80 (1987).

16 Sirota, A. *et al.*, Entrainment of neocortical neurons and gamma oscillations by the hippocampal theta rhythm. *Neuron* 60 (4), 683-697 (2008).

17 Palchykova, S., Winsky-Sommerer, R., Meerlo, P., Durr, R., & Tobler, I., Sleep deprivation impairs object recognition in mice. *Neurobiol Learn Mem* 85 (3), 263-271 (2006).

18 Tobler, I. & Borbely, A.A., Sleep EEG in the rat as a function of prior waking. *Electroencephalogr Clin Neurophysiol* 64 (1), 74-76 (1986).

19 Vyazovskiy, V.V., Cirelli, C., Pfister-Genskow, M., Faraguna, U., & Tononi, G., Molecular and electrophysiological evidence for net synaptic potentiation in wake and depression in sleep. *Nat Neurosci* 11 (2), 200-208 (2008).

20 Hanlon, E.C., Faraguna, U., Vyazovskiy, V.V., Tononi, G., & Cirelli, C., Effects of skilled training on sleep slow wave activity and cortical gene expression in the rat. *Sleep* 32 (6), 719-729 (2009).

21 Whishaw, I.Q. & Pellis, S.M., The structure of skilled forelimb reaching in the rat: a proximally driven movement with a single distal rotatory component. *Behav Brain Res* 41 (1), 49-59 (1990).

22 Rioult-Pedotti, M.S., Friedman, D., & Donoghue, J.P., Learning-induced LTP in neocortex. *Science* 290 (5491), 533-536 (2000).

23 Vyazovskiy, V.V. & Tobler, I., Handedness leads to interhemispheric EEG asymmetry during sleep in the rat. *J Neurophysiol* 99 (2), 969-975 (2008).

24 Doran, S.M., Van Dongen, H.P., & Dinges, D.F., Sustained attention performance during sleep deprivation: evidence of state instability. *Arch Ital Biol* 139 (3), 253-267 (2001).

25 Ji, D. & Wilson, M.A., Coordinated memory replay in the visual cortex and hippocampus during sleep. *Nat Neurosci* 10 (1), 100-107 (2007).

26 Luczak, A., Bartho, P., Marguet, S.L., Buzsaki, G., & Harris, K.D., Sequential structure of neocortical spontaneous activity in vivo. *Proc Natl Acad Sci U S A* 104 (1), 347-352 (2007).

27 Kuffler, S.W., Fitzhugh, R., & Barlow, H.B., Maintained activity in the cat's retina in light and darkness. *J Gen Physiol* 40 (5), 683-702 (1957).

28 Vyazovskiy, V.V., Faraguna, U., Cirelli, C., & Tononi, G., Triggering slow waves during NREM sleep in the rat by intracortical electrical stimulation: effects of sleep/wake history and background activity. *J Neurophysiol* 101 (4), 1921-1931 (2009).

29 Molle, M., Marshall, L., Gais, S., & Born, J., Grouping of spindle activity during slow oscillations in human non-rapid eye movement sleep. *J Neurosci* 22 (24), 10941-10947 (2002).

30 Steriade, M., Nunez, A., & Amzica, F., Intracellular analysis of relations between the slow (< 1 Hz) neocortical oscillation and other sleep rhythms of the electroencephalogram. *J Neurosci* 13 (8), 3266-3283 (1993).

31 Amzica, F. & Steriade, M., Electrophysiological correlates of sleep delta waves. *Electroencephalogr Clin Neurophysiol* 107 (2), 69-83 (1998).

32 Destexhe, A., Contreras, D., & Steriade, M., Spatiotemporal analysis of local field potentials and unit discharges in cat cerebral cortex during natural wake and sleep states. *J Neurosci* 19 (11), 4595-4608 (1999).

33 Steriade, M. & Amzica, F., Slow sleep oscillation, rhythmic K-complexes, and their paroxysmal developments. *J Sleep Res* 7 Suppl 1, 30-35 (1998).

34 Haider, B., Duque, A., Hasenstaub, A.R., & McCormick, D.A., Neocortical network activity in vivo is generated through a dynamic balance of excitation and inhibition. *J Neurosci* 26 (17), 4535-4545 (2006).

35 Tolias, A.S. *et al.*, Recording chronically from the same neurons in awake, behaving primates. *J Neurophysiol* 98 (6), 3780-3790 (2007).

36 Lewicki, M.S., A review of methods for spike sorting: the detection and classification of neural action potentials. *Network* 9 (4), R53-78 (1998).

37 Minagawa, A., Tagawa, N., & Tanaka, T., SMEM algorithm is not fully compatible with maximum-likelihood framework. *Neural Comput* 14 (6), 1261-1266 (2002).

38 Ueda, N., Nakano, R., Ghahramani, Z., & Hinton, G.E., SMEM algorithm for mixture models. *Neural Comput* 12 (9), 2109-2128 (2000).